Wetting-induced anisotropic structure at the interface of a glass and a sponge phase

M. Magalhães,[1] A. M. Figueiredo Neto,[1] and P. Tolédano[1,2]
[1]*Instituto de Física, Universidade de São Paulo, Caixa Postal 66318, 05315-970, São Paulo, SP, Brazil*
[2]*Groupe Structure des Matériaux Sous Conditions Extrêmes, SNBL/ESRF, 38043 Grenoble Cedex, France*
(Received 6 December 1999)

Wetting a glass surface with a sponge phase is shown to induce an anisotropic, presumably lamellar, interface structure. This static effect, and the corresponding induced birefringence measurements, are described in the framework of a theoretical phase diagram involving the sponge and lamellar phases, and taking into account a surface field and the existence of a transition between two, direct and inverted, sponge regions.

PACS number(s): 68.10.−m, 64.70.Md, 82.70.−y

Supramolecular assemblies of surfactant molecules in solution can organize themselves either with long-range order (liquid crystalline and crystal phases) or only with short-range correlation (isotropic liquid phases). In this latter case, definite identification of the local structure is difficult to achieve, especially when the aggregation process leads to the formation of amphiphilic films of macroscopic extension. A typical example is the so-called sponge (L_3) phase of surfactant solutions, whose present understanding of the structure and properties have been obtained from alternate and intricate progresses in experimental observations and theoretical considerations [1,2].

In contrast to the often adjacent lamellar (L_α) phase, which consists of a regular stack of parallel infinite bilayers, the L_3 phase is not long-range ordered, and the experimental observations point toward a microstructure where a surfactant bilayer of multiply connected topology separates two solvent domains over macroscopic distances. The most spectacular property of the sponge phase is to be flow birefringent, i.e., under velocity gradient a transient flow birefringence occurs that relaxes with a characteristic time depending on the system and its dilution. This has led to the investigation of various kinds of shear effects produced with sponge phases, among which the shear on lamellar order has been the most studied [3,4]. Recently, evidences of shear induced sponge-to-lamellar transition [5] above some critical shear rate [6], have been demonstrated experimentally.

The preceding effects are of dynamical nature. We report on a static effect that consists in inducing an anisotropic structure at the interface between a glass surface and a sponge phase. Measuring the magnitude of this wetting effect for different compositions of the sponge phase, provides an insight into the variation of the local anisotropy of the sponge phase. Our proposed interpretation assumes a surface-field induced phase transition from the sponge phase to an interface anisotropic phase.

The lyotropic system investigated is a mixture of sodium dodecyl sulfate (SDS)/1-pentanol (POH)/cyclohexane $C_6H_{12}(C_6)$/water (W). The phase diagram of this quaternary system was already explored for different concentrations of the components [7,8], and a sponge phase was identified in the C_6-rich-W-poor corner of a ternary phase diagram. In the phase diagram constructed in the present paper the experimental points have been obtained by varying all the components of the mixture. The phases were identified using the same optical microscopy, x-ray scattering, and diffraction setup described in Ref. [9], and for the identification of the sponge phase, the same flow-induced birefringence apparatus depicted in Ref. [9]. The phase boundaries of the sponge phase are shown in the ternary phase diagram of Fig. 1. The phase has an elongated shape, almost parallel to the water side of the triangular phase diagram, in a narrow interval of concentrations of SDS+POH, around the average concentration $[\mathrm{SDS+POH}]\simeq 7.5$ mol%, where [ ] designates the molar fraction, with $[\mathrm{SDS}]/[\mathrm{POH}]=0.17$. It extends in the intervals (in mol %): $8\lesssim[C_6]\lesssim 75$ and $23\lesssim[W]\lesssim 89$. With increasing concentration of SDS+POH one finds around the average concentration $[\mathrm{SDS+POH}]\simeq 15$ mol% the direct (L_1) and inverted (L_2) isotropic micellar phases, corresponding, respectively, to the W-rich and C_6-rich sides of the phase diagram. The L_1 and L_2 regions seem to form a single phase with a continuous crossover between the direct and inverted micellar configurations. At lower concentrations of $[\mathrm{SDS + POH}] \lesssim 5$ mol%, one finds the infinite lamellar (L_α) phase mixed with L_1 or L_2, which extends from the water-rich corner ($[W]\simeq 92$ mol%) to the water-poor corner ($[W]\simeq 10$ mol%).

Two optically distinct regions were found for the sponge phase, one almost transparent and one light diffusive, respectively, located below and above a line determined by the

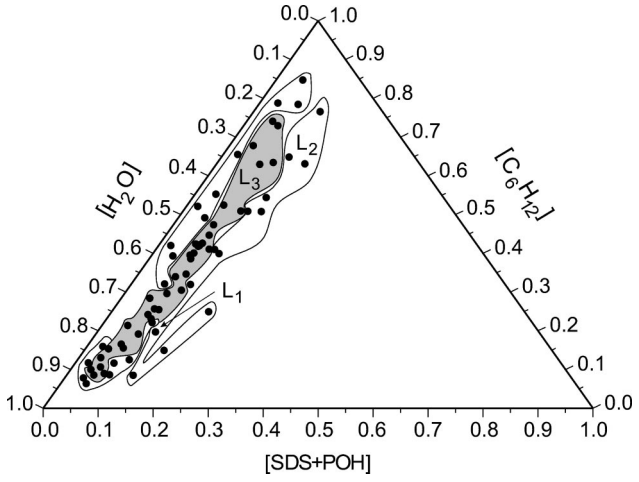

FIG. 1. Ternary representation of the phase diagram of the lyotropic mixture SDS/POH/C_6H_{12}/H_2O at 21.5 °C. Solid circles represent the experimental points.

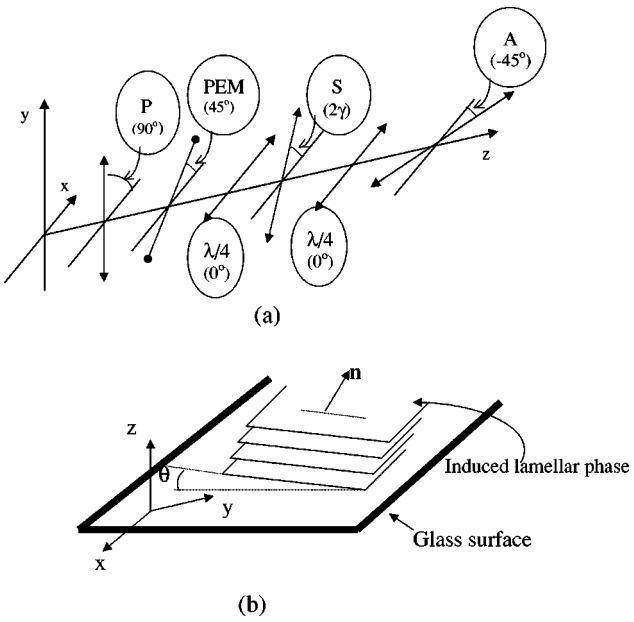

FIG. 2. (a) Sketch of the experimental setup. P, A, λ/4, *S*, and PEM are the polarizer, analyzer, quarter-wave plate, the sample, and the photoelastic modulator, respectively. The numbers indicate the orientation angles with respect to the *x* axis of the laboratory reference axes. (b) Sketch of the glass plate and of the induced lamellar phase with the optical axis (**n**) tilted by an angle θ with respect to the *z* axis. 2γ represents the angle between the projection of **n** in the $x-y$ plane, and the *x* axis.

concentrations $[C_6] \simeq 23$ mol % and $[W] \simeq 68$ mol %. Taking into account the respective neighboring of the L_1 and L_2 phases, as well as the results of viscosity measurements [10], this behavior can be presumably attributed to a crossover from inverted to direct configurations, i.e., to the transition between direct and inverted sponge phases.

The setup used to measure the surface-field induced birefringence is represented in Fig. 2(a). It consists [11] in a polarized HeNe laser beam, two quarter-wave plates, an optical modulator with an antireflecting coating, and an analyzer. The first and second harmonics of the sample transmittance are measured with two lock-in amplifiers. The glass (Hellma) cells in which the sample is placed are composed of two parts, one of them has a cavity with different thicknesses of 0.2, 0.5, and 0.9 mm, made by a spacer which keeps the sample thickness, and a cover glass. The temperature is kept fixed at 21.5 °C. The sample mixture is poured inside the glass cell 48 h after prepared. The measured sample optical phase shift is corrected by the residual phase shift introduced by the glass cell [12]. The residual glass phase shift (Ψ_g) is measured independently with the empty sample holder. In the case of the 0.5 mm thick cell $\Psi_g = (0.035 \pm 0.004)$ rad. A model of a pile of birefringent layers (glass+liquid-crystal layer) is used to obtain the optical phase shift Ψ and the optical axis direction γ of the sample itself (without the residual glass contribution), with respect to the horizontal axis [Fig. 2(a)]. To verify the possible influence of the sample thickness on the measured values of Ψ, different sample holders with different spacers (0.2, 0.5, and 0.9 mm) were used. The values of Ψ obtained with a L_3 sample ($[C_6] \simeq 47$ mol %) are: $\Psi_{0.2} = (0.05 \pm 0.01)$ rad; $\Psi_{0.5} = (0.066 \pm 0.006)$ rad, and $\Psi_{0.9} = (0.063 \pm 0.006)$ rad, respectively.

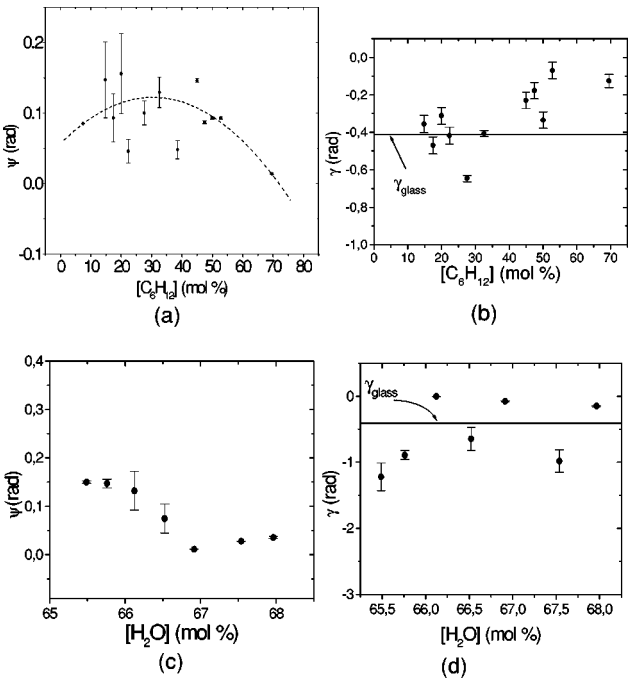

FIG. 3. Optical phase shift Ψ (a) and tilt angle γ (b) as a function of $[C_6H_{12}]$ at fixed concentration of [SDS+POH]= 7.5 mol %, with [SDS]/(POH)=0.17. Optical phase shift (c) and tilt angle (d) as a function of $[H_2O]$, at fixed concentration of $[C_6H_{12}] = 25.4$ mol %. The parabola in (a) is a best fit result. The horizontal lines in (b) and (d) indicate the tilt angle of the glass plate.

These results clearly indicate that the (sample) induced phase shift measured is not due to a bulk effect, i.e., the procedure of filling the sample holder is not at the origin of the induced birefringence effect. All the results presented hereafter refer to the 0.5 mm thick sample holder.

Figure 3(a) shows the dependence of Ψ on the molar concentration of C_6 for values of $[C_6]$ corresponding to the sponge phase, along a parallel to the water side of the phase diagram for [SDS+POH]=7.5 mol %. The Ψ average curve has a parabolic shape with a downward concavity and a maximum located around $[C_6]_{max} \simeq 25$ mol %. Below $[C_6]_{max}$ the values of Ψ appear as more randomly distributed on both sides of the curve. The optical axis direction γ measured in function of $[C_6]$ [Fig. 3(b)] shows below $[C_6]_{max}$ a coincidence with the optical axis of the glass plate, and above $[C_6]_{\max}$ a deviation from the preceding direction.

Another series of measurements were made in order to estimate the variation of Ψ and γ along a segment of the phase diagram crossing transversely the sponge phase, and corresponding to $[C_6] \simeq 25.4$ mol %, and $65.5 \leqslant [W] \leqslant 68$ mol %. The Ψ versus $[W]$ dependence shown in Fig. 3(c) indicates that with decreasing values of $[W]$, Ψ decreases linearly down to $\Psi \gtrsim 0$ for $[W] \simeq 66.8$ mol %, then increases up to $\Psi = 0.16$ rad. The corresponding γ versus $[W]$ curve [Fig. 3(d)] shows a random distribution of the γ values around an average value coinciding with the direction of the optical axis of the glass plate.

The preceding results yield the following observations: (1) Ψ takes for all the experimental points a nonzero value expressing an induced birefringence resulting from wetting the glass surface by the sponge phase. Along the ''long

axis'' of the sponge phase the induced birefringence reaches its maximum nearby the presumed crossover from direct-to-reversed sponge phase. Along the ''short axis'' of the sponge phase domain, the induced birefringence decreases when going from the border of the phase, which is close to the (lamellar + L_1) region, to the border, which is close to the isotropic micellar phase (L_1). (2) The induced birefringence effect reflects the existence of an anisotropic interface structure between the cover glass and the bulk of the sponge phase. The variation of the γ angle along the long axis of the L_3 region, shows that for the direct sponge phase the axis of the anisotropic structure coincides with the optical axis of the glass plate, and that it deviates progressively from the preceding direction when going through the inverted sponge phase region. Along the short axis of the direct sponge phase region, the axis of the induced anisotropic structure coincides, in average, with the optical axis of the glass plate. (3) The preceding features are consistent with an induced lamellar structure for the anisotropic phase, with the axis perpendicular to the lamellas tilted with respect to the normal to the glass surface, as shown in Fig. 2(b). The formation of lamellas at the surface of the sponge phase can be understood in terms of a surface field-induced segregation process: The molecules of SDS+POH are the only amphiphilic molecules in the mixture and therefore their polar heads are in contact with the glass surface together with hydration water molecules. Under wetting, the polar heads are attracted by the ions present on the glass surface, rejecting the solvent molecules ($W+C_6$) inside the bulk. Consequently, the concentration of SDS + POH will increase close to the surface inducing the segregated lamellar phase.

An interpretation of our results requires to insert them in the theoretical phase diagram, which contains a sponge-lamellar phase transition and a crossover between the direct and inverted sponge regions. Assuming a parent sponge phase of isotropic symmetry, the relevant two order parameter free-energy will be taken as

$$\Phi(\eta,\zeta,x)=\Delta\mu\zeta+\frac{\zeta^2}{2}+\frac{(x-x_c)}{2}\eta^2+\frac{a}{3}\eta^3+\frac{\eta^4}{4}+\delta\eta^2\zeta, \tag{1}$$

$\zeta=\rho-\rho_c$, where ρ is a dimensionless concentration order parameter defined by

$$\rho=\frac{[W]-[C_6]}{[W]+[C_6]}$$

and varying in the phase diagram of Fig. 1 between $\rho_{min}\simeq-0.53$ and $\rho_{max}\simeq 0.83$. $\rho_c\simeq 0.49$ is the critical value of ρ at the direct-inverted sponge phase transition ($[W]\simeq 68,[C_6]\simeq 23$). $\Delta\mu=(\mu_{C_6}-\mu^{\circ}_{C_6})-(\mu_W-\mu^{\circ}_W)$, where μ_{C_6} and μ_W are the chemical potentials for C_6 and W for the solution, and $\mu^{\circ}_{C_6},\mu^{\circ}_W$ the corresponding quantities for the independent fluids. x=[SDS+POH], and x_c is a critical value of x corresponding to the limit of stability of the sponge-lamellar transition on the line $\rho=\rho_c$. η represents the segregation order parameter associated with the isotropic liquid to lamellar transition. a and δ are negative constant coefficients. Denoting σ the surface field conjugate to η, one has the constraint

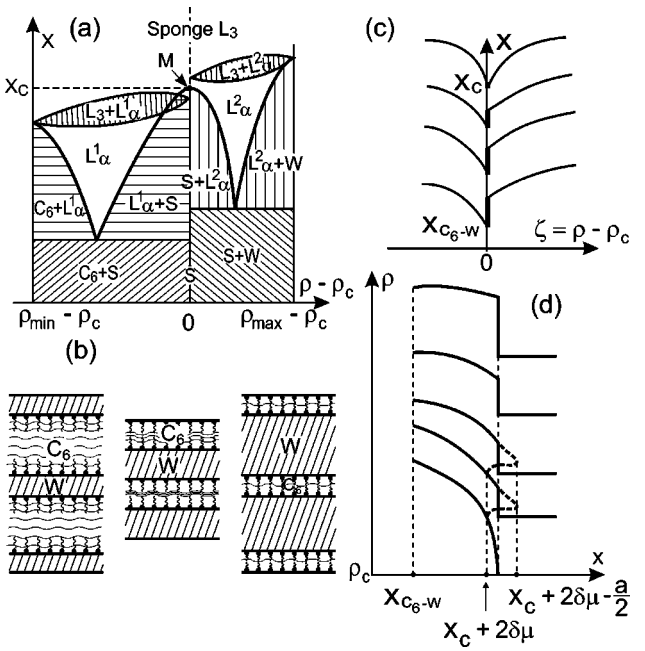

FIG. 4. (a) Theoretical $x(\rho-\rho_c)$ phase diagram associated with $\Phi(\eta,\zeta,x)$ [Eq. (1)], and described in the text. (b) From left to right: possible configurations of the L^1_α, S, and L^2_α phases. (c) Dependence of η^{L_α} on ζ for different values of $x_{C_6-W}\leqslant x\leqslant x_c$. (d) Dependence of η^{L_α} on x for the L^1_α region for different values $\rho_S\leqslant\rho\leqslant\rho_c$.

$$\sigma_e=(x-x_c)\eta_e+a\eta_e^2+\eta_e^3+2\delta\eta_e\zeta \tag{2}$$

showing that the equilibrium value η_e of the segregation order parameter is determined by the magnitude of the (constant) surface field σ_e, which represents the effect of the glass plate.

At constant chemical potentials and variable ρ and x, the equations of state resulting from a minimization of Φ with respect to ζ and η are

$$\zeta=-\Delta\mu-\delta\eta^2 \quad \text{and} \quad \eta[(x-x_c)+a\eta+\eta^2+2\delta\zeta]=0. \tag{3}$$

Equation (3) and the stability condition: $(x-x_c)+2a\eta+(3-4\delta^2)\eta^2+2\delta\zeta\geqslant 0$, allows us to construct the phase diagram shown in Fig. 4(a). It shows the following equilibrium properties.

(1) The line $\rho=\rho_c$ divides the phase diagram into two similar regions in which two distinct lamellar phases, denoted L^1_α and L^2_α are surrounded by regions of coexistence with other phases. Figure 4(b) illustrates the most probable configurations of the L^1_α and L^2_α phases in the C_6-rich and W-rich sides of the phase diagram. Hence, L^1_α is formed by the intercalation of thin W layers and thick amphiphilic layers, in which the C_6 molecules predominate in the central part of each layer, and L^2_α corresponds to the inverted geometry. The S phase, shown in Fig. 4(b) is stabilized at $\rho=\rho_c$, below the regions of stability of L^1_α and L^2_α. It displays a smectic-type layer periodicity requiring equivalent amounts of W and C_6, consistent with the value $\rho_c=0.49$.

(2) The sponge phase L_3 corresponds to the equilibrium order-parameter values $\eta^{L_3}=0$ and $\zeta^{L_3}=-\Delta\mu$. It is

stable for $x \geqslant x_{L_3-L_\alpha} = x_c + 2\delta\Delta\mu$. The limit of stability lines $x[\rho(x_{L_3-L_\alpha})]$ coincide with the lower boundaries of two disconnected cigar-shaped regions of coexistence with the L_α^1 and L_α^2 phases. The left- and right-handed coexistence regions are located, respectively, below and above the *M*-point corresponding to $x = x_c$ and $\rho = \rho_c$. At this three-phase point, at which merge the L_α^1, L_α^2, and L_3 phases, one goes continuously from the sponge phase to the region of coexistence of the L_1^α, L_2^α, and *S* phases.

(3) The L_α^1 and L_α^2 phases take place across first-order transitions from the L_3 phase, and correspond to the equilibrium order parameters:

$$\zeta_{L_\alpha} = -\Delta\mu - \delta(\eta^{L\alpha})^2$$

$$\text{with} \quad \eta^{L\alpha} = \frac{a}{2\epsilon} + \left\{ \left(\frac{a}{2\epsilon} \right)^2 + \left[\frac{(x-x_c) - 2\delta\Delta\mu}{\epsilon} \right] \right\}^{1/2}, \quad (4)$$

where $\epsilon = 2\delta^2 - 1$. The lamellar phases are bounded upward by the upper boundaries of the cigar-shaped regions. With decreasing *x*, the L_α^1 and L_α^2 phases are bounded downward by the $C_6 + S$ and $S + W$ solutions.

When going across the $\rho = \rho_c$ line, at fixed *x*, from the L_α^1 to the L_α^2 regions of stability, $\eta^{L\alpha}(\zeta)$ undergoes an upward jump, the magnitude of which is determined by $(x - x_c)$. Figure 4(c) represents the $\eta^{L\alpha}(\zeta)$ curves for different values of *x*. It shows that $\eta^{L\alpha}$ increases with increasing values of $|\rho - \rho_c|$ and decreases when $|\rho - \rho_c| \to 0$, expressing the property of the lamellar phase to ''soften'' when ρ gets closer to ρ_c. In other words, the *spontaneous* birefringence, which is expressed by $\eta^{L\alpha}$, *decreases* when going from ρ_{max} or ρ_{min} to ρ_c. Since the surface field σ_e imposed by the glass plate determines a *constant* value for η_e [Eq. (2)], the *induced* birefringence $\eta_e - \eta^{L\alpha}$ will *increase* when approaching ρ_c from ρ_{max} or ρ_{min}, as found in Fig. 3(a). The curve of Fig. 3(b) can be interpreted by the property of the L_α^1 and L_α^2 lamellar phases to display slightly different orientations.

Figure 4(d) shows the dependence of $\eta^{L\alpha}$ on *x* within the L_α^1 region for different values of $\rho_S \leqslant \rho \leqslant \rho_c$, where ρ_S coincides with the merging point of L_α^1 with the $C_6 + S$ solution. Except at $\rho = \rho_c$, $\eta^{L\alpha}(x)$ exhibits an upward jump at the $L_3 \to L_\alpha^1$ transition, the magnitude of which increases when $\rho \to \rho_S$. Below the transition the total spontaneous birefringence increases with decreasing *x* in the region of coexistence with the *S* phase, due to the additional contribution of this latter phase to the segregation process. This will result in a correlated decrease of the measured birefringence for the wetting induced lamellar phase, as illustrated in Fig. 3(c). The average distribution of points in Fig. 3(d) reflects a single orientation coinciding with the axis of the glass plate.

In summary we have reported experimental evidences of an anisotropic phase induced by wetting a glass surface with a sponge phase. This new effect has been interpreted using a theoretical phase diagram involving the sponge-to-lamellar transition, and taking into account the existence of direct and inverted sponge regions suggested by the optical observations. Our proposed interpretation needs to be supported by further experiments confirming the lamellar nature of the induced anisotropic phase, and disclosing the properties of the sponge and anisotropic phases at the crossover between the direct and inverted regimes.

Fundação de Amparo à Pesquisa do Estado de São Paulo supported this work.

[1] D. Roux, C. Coulon, and M.E. Cates, J. Phys. Chem. **96**, 4174 (1992).
[2] G. Porte, J. Phys.: Condens. Matter **4**, 8649 (1992).
[3] O. Diat and D. Roux, Langmuir **11**, 1392 (1995).
[4] D. Antelmi, P. Kekicheff, and P. Richetti, J. Phys. II **5**, 103 (1995).
[5] C. Quilliet, C. Blanc, and M. Kleman, Phys. Rev. Lett. **77**, 522 (1996).
[6] H.F. Mahjoub *et al.*, Phys. Rev. Lett. **81**, 2076 (1998).
[7] P. Fabre *et al.*, Phys. Rev. Lett. **64**, 539 (1990).
[8] C. Quilliet, P. Fabre, and V. Cabuil, J. Phys. Chem. **97**, 287 (1993).
[9] M. Magalhães *et al.*, J. Chem. Phys. **108**, 3835 (1998).
[10] M. Magalhães *et al.* (unpublished).
[11] P.L. Frattini and G.G. Fuller, J. Rheol. **28**, 61 (1984).
[12] C.Y. Matuo *et al.*, Phys. Rev. E **56**, R1310 (1997).